Applied Catalysis B: Environmental 328 (2023) 122506

Contents lists available at ScienceDirect

Applied Catalysis B: Environmental

journal homepage: www.elsevier.com/locate/apcatb

Dynamic confinement catalysis in Fe-based CO_2 hydrogenation to light olefins

Linkai Wang [a,b], Yu Han [a], Jian Wei [a], Qingjie Ge [a,*], Shijian Lu [c,d,*], Yanpeng Mao [e], Jian Sun [a,*]

[a] Dalian National Laboratory for Clean Energy, Dalian Institute of Chemical Physics, Chinese Academy of Sciences, Dalian 116023, China
[b] University of Chinese Academy of Sciences, Beijing 100049, China
[c] Jiangsu Key Laboratory of Coal-based Greenhouse Gas Control and Utilization, China University of Mining and Technology, Xuzhou, Jiangsu 221008, China
[d] Carbon Neutrality Institute, China University of Mining and Technology, Xuzhou, Jiangsu 221008, China
[e] National Engineering Laboratory for Reducing Emissions from Coal Combustion, Shandong Key Laboratory of Energy Carbon Reduction and Resource Utilization, School of Energy and Power Engineering, Shandong University, Jinan 250061, China

ARTICLE INFO

Keywords:
CO_2 hydrogenation
Light olefin
MOR
Diffusion
Dynamic confinement

ABSTRACT

Hydrogenation of CO_2 into light olefins is an important route to carbon neutrality. Most of traditional researches focus on the catalyst component, structure, and promoter to enhance the selectivity of light olefins while ignoring the diffusion of products. Here, we report a NaFeZr-MOR composite catalyst for light olefin synthesis in CO_2 hydrogenation via pore confinement. The selectivity in hydrocarbons and STY (Space-time yields) of $C_{2-4}^{=}$ is gradually increasing maximum up to 51.3% and 12.2 ($mmol \cdot g_{cat}^{-1} \cdot h^{-1}$), which lie in a high level among reported Fe-based catalysts. Further characterization revealed that the essence of selectivity change period is the accumulation and evolution of carbonaceous species, which causes the change of product diffusion behavior. It suppresses the escape of heavy hydrocarbons from MOR pores, leading to an increased light olefin, especially ethylene, which is called "dynamic confinement". These findings provide a new insight for controlling low-carbon product selectivity in CO_2 hydrogenation.

1. Introduction

Due to the development of the social economics, excessive CO_2 emissions into the atmosphere has caused huge climate problem. However, the CO_2 has also turned out to be an effective carbon resource to produce high value-added chemicals [1,2]. The CCUS proposed in recent years has attracted more and more attention [3–6]. Light olefins ($C_{2-4}^{=}$) are mainly used in the production of plastics, rubbers, lubricants and other daily necessities [7,8]. They are the basic building blocks of the chemical industry. With the development of economy, the demand for light olefins is growing, however, the way to obtain light olefins from traditional fossil resources such as petroleum and coal is becoming increasingly unsustainable, while the production of light olefins from CO_2 coupling with green hydrogen produced from renewable energy is a green and promising route [9–11].

It is generally accepted that there are two routes for CO_2 hydrogenation technology, namely, the Fischer-Tropsch route with CO as the intermediate (FTO) and the methanol route with CH_3OH as the intermediate (MTO) [12]. Considering industrial prospect and cost of the technical route, Fe-based F-T route are extensively studied and relatively high activity for both the RWGS and FTS reactions of iron, especially in olefin synthesis [13,14]. For the FTO route, the selectivity of products is limited by the ASF distribution, the selectivity of light hydrocarbons (C_2-C_4) can only reach 58%. Researchers have focused on catalyst design, such as promoters, adding the second active metal, building special structure to break the ASF distribution [15]. These catalysts are aiming to regulate the active sites to improve the selectivity, while ignoring that the catalytic reaction is also including the diffusion. Previous researches show that the diffusion process has an important influence on the products distribution of C1 catalysis [15]. Hence, more studies conducted to improve the selectivity of light olefins in CO_2 hydrogenation by using the confinement structure of catalysts [16–20]. Recently, Wu et al. reported a honeycomb-structure graphene as the support, using the advantages of $C_{2-4}^{=}$, such as fast mass transfer,

* Corresponding authors.
* Corresponding author at: Jiangsu Key Laboratory of Coal-based Greenhouse Gas Control and Utilization, China University of Mining and Technology, Xuzhou, Jiangsu 221008, China.
E-mail addresses: geqj@dicp.ac.cn (Q. Ge), lushijian@cumt.edu.cn (S. Lu), sunj@dicp.ac.cn (J. Sun).

https://doi.org/10.1016/j.apcatb.2023.122506
Received 12 January 2023; Received in revised form 13 February 2023; Accepted 20 February 2023
Available online 21 February 2023

avoiding over secondary hydrogenation, the selectivity of light olefins was increased to 59% [21].

In recent years, the zeolite of bifunction catalysts have attracted more attention because of its shape selective to regulate the product distribution [22]. For example, SAPO-34 [23–25] for the light olefins production due to its 8-MR structure; MOR [26–28] with 8-MR side pocket is favorable for ethylene formation; ZSM-5 [12,29–31], SAPO-11 and ZSM-22 [32], which the 10-MR and 12-MR are beneficial to gasoline hydrocarbons. In addition, the sheet ZSM-5 with lower b/a axis ratio is more easy to form aromatic hydrocarbons without affecting the selectivity of light molecules, research shows that the structure is favorable for the diffusion of aromatic compounds [33]. Previous studies revealed the complex carbonaceous species in the zeolite after CO_2 hydrogenation through solid-state nuclear magnetic resonance (ssNMR) technology and proposed the hydrocarbon pool mechanism similar to the MTH process [34], indicating the complex evolutions of carbonaceous species in the zeolite during reaction process [35]. However, these findings are still based on the analysis of the static species after reaction. The dynamic evolution of carbonaceous species during reaction and its influence on the diffusion behavior are still unclear.

Here, we report a Fe-based composite catalyst coupled with MOR zeolite (NaFeZr-MOR) for CO_2 hydrogenation to light olefins. During the selectivity change period in CO_2 hydrogenation, the accumulation of carbonaceous species in the support and zeolite channel can create a dynamic confinement for the products, which ultimately enhances the selectivity of light olefins, making it lie in a high level among reported literatures, as shown in Fig. S1. Due to the differences in the size of product molecules and its diffusion, the production of heavy C_{5+} is inhibited. As mentioned above, MOR and SAPO-34 zeolites were given more attention in our study. Especially for MOR, its unique 8-MR side pocket is more favorable for ethylene production. At the same time, more zeolites with microporous sizes in addition to MOR could be extended based on these findings.

2. Experiment section

2.1. Catalyst preparation

2.1.1. Chemicals

ZrO_2(NaiOu, Co. Ltd, China) and α-Al_2O_3(HengGe, Co. Ltd, China), MOR (AoSi, Co. Ltd, China, Si/Al=16.7), SBA-15 (Aladdin, Co. Ltd, China), SAPO-34 (Si/Al=0.217), ZSM-5 (Si/Al=27). SAPO-34 and ZSM-5 were purchased from Nankai University Catalyst Company. Hydrothermally synthesized mesoporous ZrO_2 (Supplementary Information for details), named HT-ZrO_2. $Fe(NO_3)_3 9H_2O$ and $NaNO_3$ (KeMiOu, Co. Ltd, China), 1-C_6H_{12} (DaTe, Co, Ltd, China). The Commercial ZrO_2 is used with its accepted state and fresh zeolite are calcined at 500 °C in air for 4 h, then granulated and sieved (20–40 mesh).

2.1.2. Catalyst preparation

The NaFeZr catalyst was prepared by the equal volume impregnation method, keeping the mass ratio of Na/Fe is 1:10. Typically, 2.1643 g Fe $(NO_3)_3 \cdot 9H_2O$ and 0.1109 g $NaNO_3$, as well as 0.3977 mL deionized water were heated to prepare a solution. Then, the above solution was dropped into the calculated 2.5310 g ZrO_2 in equal volume, stirred thoroughly and then sonicated for 15 min, followed stand for 12 h. Then, after drying at 110 °C in air for 10 h, calcined in air at 450 °C for 4 h, cooled and granulated and sieved (20–40 mesh). When the supports were α-Al_2O_3, SBA-15, and HT-ZrO_2, like the above process, named NaFeX (X = Al, Si) and NaFeZr (HT). The NaFeZr (Blockage) catalyst was prepared by first impregnating ZrO_2 with ZrO_2 in equal volume, named ZrO_2 (Blockage) as a support, and then impregnating ZrO_2 (Blockage) with Na and Fe in equal volume, keeping the mass ratio of Na/Fe as 1:10, the treatment procedure was the same as the NaFeZr catalyst above, named NaFeZr (Blockage).

Based on the work by our group reported previously [12], the NaFeZr-MOR composite catalysts are filled by Dual-bed, Granule-stacking, Powder-mixing, etc. Named NaFeZr-MOR, NaFeAl-MOR, NaFeZr-ZSM-5 and so on, collectively known as NaFeX-ZEO series; The shielding operation of the B-acid sites of the 8-MR on MOR is operated with reference to the literature [36], named Ex-8-MOR (Supplementary Information for details). The catalysts prepared by the coprecipitation method are previously reported by our group [37], and coupled with MOR in a dual-bed structure, named NaFe and NaFe-MOR, respectively.

2.2. Catalyst characterization

Nitrogen adsorption-desorption isotherms were obtained at − 196 °C on a Quantachrome QUADRASORB SI and AUTOSORB iQ_2 instrument, the sample was pretreated under vacuum at 300 °C for 4 h, the specific surface area, pore size and pore volume were calculated based on Brunauer-Emmett-Teller (BET), Barret-Joyner-Halenda (BJH), and t-plot method, respectively.

X-ray diffraction (XRD) patterns spectra were obtained on a PANalytical X'pert Pro diffractometer equipped with Cu Kα radiation, (λ = 1.5418 Å), operated at 40 kV and 40 mA.

Transmission Electron Microscope (TEM) images were obtained on a FEI Talos 200x system with the acceleration voltage of 200 kV.

Temperature-Programmed-Hydrogenation (TPH) was performed on a BELCATII instrument equipped with a thermal conductivity detector (TCD) and a Pfeiffer OmniStar Mass Spectrometer (MS). Typically, 100 mg sample was pretreated under a flowing He at 300 °C for 1 h. After cooling down to 50 °C and was purged under a H_2 flowing for 0.5 h, the sample started to increase temperature from 50 °C to 900 °C at a heating rate of 10 °C/min, meanwhile, the TCD signal was recorded and products sign of m/z = 16 was recorded by online MS.

The Fourier transform infrared spectroscopy of pyridine-adsorbed (Py-IR) was performed on a Brukers Optics XF808–04 spectrometer, all spectra were recorded within a range from 4000 to 1200 cm^{-1}. Typically, the samples were pressed to a round sheet (about 15 mg, 12 mm) before put them into the sample cell. The sample was pretreated at 450 °C for 1 h under the vacuum to clear the absorbed species, then cooled to the room temperature and recorded a background spectrum. Subsequently, the sample was exposed to the flowing of pyridine at room temperature until saturation. Finally, the spectrum was recorded below 35 °C after vacuum treatment for 30 min at 150 °C and 350 °C, respectively. All difference spectra were obtained by subtracting the background spectrum obtained above.

In situ DRIFT was performed on a Nicolet iS50 spectrometer (ThermoFisher Scientific, USA). Typically, the catalyst was carefully transferred into the Praying mantis in situ cell (Harrick Scientific Product). Before *In situ* DRIFT experiment, the catalyst was purged by H_2 flow (25 mL min^{-1}) for 30 min at room temperature, then, the catalyst started to increase temperature from room temperature to 400 °C at a heating rate of 5 °C/min and later keep stable for 30 min. Subsequently, cooling to 320 °C and switching to feed gas (CO_2: H_2: N_2 =24 v%: 72 v%: 4 v%), starting scanning, 10 min every time.

The carbonaceous deposition in zeolites were analyzed by the gas chromatography-mass spectrometry (GC-MS, Agilent 8890–7250) equipped with a PONA capillary column and a flame ionization detector (FID). Typically, the spent zeolites were dissolved by the HF acid solution (20%), the hydrocarbons solutes were extracted by CH_2Cl_2 and then analyzed by the GC-MS.

2.3. CO_2 hydrogenation test

CO_2 hydrogenation test reaction of all catalysts were performed on a stainless steel fixed-bed reactor with an inner diameter of 14 mm. Typically, for the NaFeX (X = Zr or Al or Si) catalyst, 0.5 g catalyst were put into the reactor; for the NaFeX-ZEO catalyst, 0.15 g NaFeX catalysts were weighed and kept the mass ratio (NaFeX: ZEO) is 1:3. Subsequently, the catalysts were reduced at 400 °C for 8 h using pure H_2 (25

mL·min^{-1}, 0.1 MPa) before CO_2 hydrogenation test reaction. After reduction, making the reactor cool to 320 °C, then switching to the feed gas (CO2: H2: N2 = 24 v%: 72 v%: 4 v%) to perform CO_2 hydrogenation reaction with continuous flowing with pressing to 3 MPa, here, the N_2 as an internal standard. The reaction conditions were 320 °C, 3 MPa, 9000 mL·g$_{cat}^{-1}$·h^{-1}(GHSV). To prevent residues, the pipeline from the reactor outlet to the gas chromatography (GC) inlet is kept at least 175 °C. Gas products were analyzed by two tandem on-line gas chromatography. One is Shimadzu GC-2014 equipped with a Thermal conductivity detector (TCD) and active charcoal column (TDX-01) for the analysis of N_2, CO, CH_4, CO_2. The other one is Shimadzu GC-2014 equipped with a flame ionization detector (FID) and capillary column (PONA) for the analysis of hydrocarbons. CO_2 conversion, CO selectivity, and hydrocarbon selectivity were calculated on a molar carbon basis:

$$CO_2 conversion(\%) = \frac{CO_{2in} - CO_{2out}}{CO_{2in}} \times 100\%$$

Where the CO_{2in} and CO_{2out} represent the moles of CO_2 at the inlet and outlet, respectively.

$$COselectivity(\%) = \frac{CO_{out}}{CO_{2in} - CO_{2out}} \times 100\%$$

Where the CO_{out} represent the moles of CO at the outlet.

The selectivity of hydrocarbons (C_i) in total hydrocarbons was obtained by the following formula:

$$C_i hydrocarbon selectivity\ (C - mol\%) = \frac{mol\ of\ C_i \times i}{\sum_{i=1}^{n} mol\ of\ C_i \times i}$$

3. Results and discussion

3.1. Selectivity change period of NaFeZr catalyst and NaFeX-ZEO catalyst

As shown in Fig. S2, the N_2 physical adsorption isotherm confirm the mesopore structures of ZrO_2 and HT-ZrO_2 (Hydrothermal), respectively. Meanwhile, ZrO_2 can also promote the activation of CO_2 and its hydrogenation [38–40]. Na is usually used as promoter in the design of CO_2 hydrogenation catalysts, which play an important role in activating CO_2 and promoting C-C coupling [41–43]. Therefore, we chose ZrO_2 and Na as the support and promoter respectively, preparing NaFeZr catalysts. As shown in Fig. 1a, the NaFeZr catalyst show the highest selectivity for $C_{2-4}^{=}$ when NaFe supported on different supports, which could be attribute to more weak metal-support interaction and superior pore size effect of ZrO_2 [44,45].

Subsequently, we further studied the performance of a single NaFeZr catalyst. Table S1 shows that the selectivity of $C_{2-4}^{=}$ increased from 41.4% to 44.1% during the selectivity change period (TOS=50 h) and later level off (Fig. 1b), while the selectivity of high carbon C_{5+} decreased from 40.7% to 35%, such change of selectivity is unique and just bring about the highest selectivity of $C_{2-4}^{=}$ for the NaFeZr compared to the other NaFeX catalysts. (Fig. 1a).

More interestingly, as shown in Table S2, this phenomenon became more pronounced when the NaFeZr catalyst was coupled with MOR in a dual-bed structure: with increasing reaction time to 50 h, the selectivity of $C_{2-4}^{=}$ grew from 0.4% to 50.3%, while the selectivity of C_{5+} grew rapidly from 13.9% to 33.7%, and then kept decreasing to 29.7%. Similarly, the selectivity of the NaFeZr-MOR composite catalyst also remained stable after selectivity change period (Fig. 1c). To further validate the universality, different conditions was set to investigate the

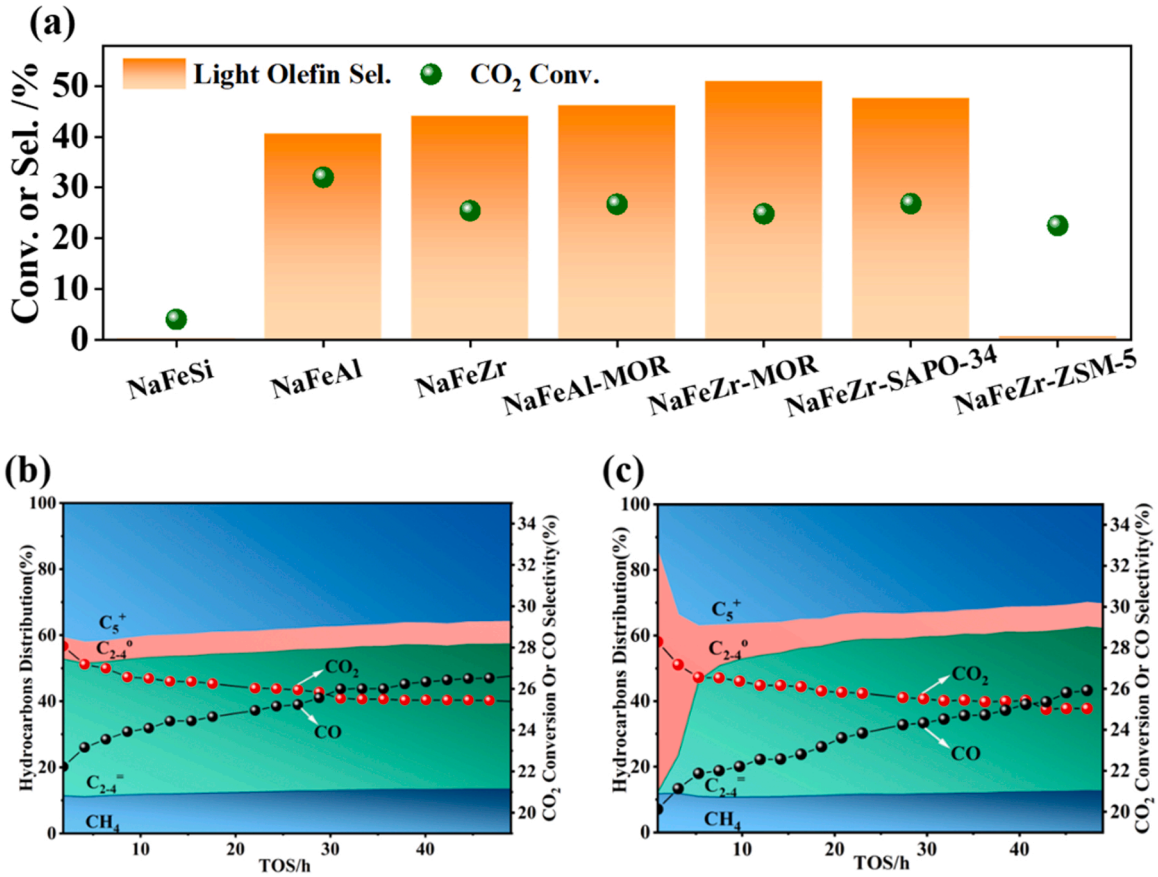

Fig. 1. Catalytic performance of NaFeX or NaFeX-ZEO catalysts (TOS=50 h) (a) and NaFeZr (b) NaFeZr-MOR (c) with time on stream. Reaction conditions: 320 °C, 3 MPa, H_2/CO_2 = 3, GHSV= 9000 mL·g$_{cat}^{-1}$·h^{-1}. ($C_{2-4}^{=}$ and C_{2-4}° represent the light olefins and light alkanes, respectively.).

NaFeX-ZEO (X = Zr,Al) series catalysts. As shown in Fig. S3, we can find that although the final selectivity of $C_{2-4}^{=}$ varies when catalysts with different supports coupled with MOR, they all have a selectivity change period, and the dynamic change pattern of product selectivity is consistent with the above. We further investigated the NaFeZr-MOR composite catalyst under different mass ratios, gas hourly space velocities (GHSV), and different configuration, the results are shown in Figs. S4-S6, which are also consistent with the aforementioned pattern. Meanwhile, we observed in Fig. S7, when NaFeZr catalyst coupled with SAPO-34 with 8-MR, a similar selectivity change period appeared, while its $C_{2-4}^{=}$ selectivity was lower than that of NaFeZr-MOR catalyst when reaching the steady state; when NaFeZr catalyst coupled with ZSM-5

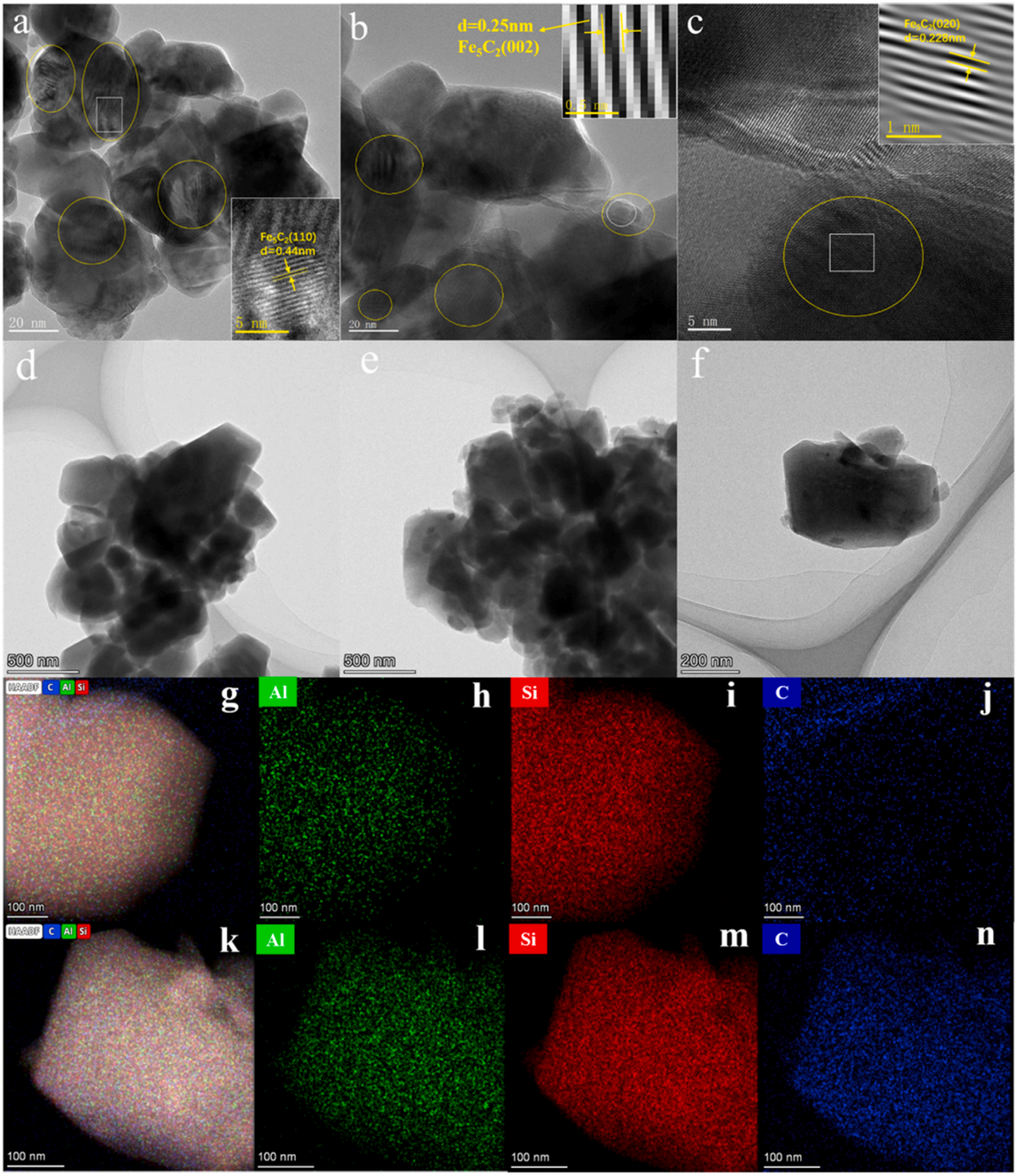

Fig. 2. High resolution TEM image. HRTEM image of spent NaFeZr catalysts (a, b, c) with IFFT analysis, and MOR of fresh (d) and spent (e, f). HAADF-TEM image of fresh MOR (g, h, i, j) and spent MOR (k, l, m, n) with EDS mapping elements analysis.

with 10-MR pores, the similar phenomenon was not observed. Such results suggest that the "selectivity change period" phenomenon closely related to the topological type and pore structure of the zeolite.

3.2. Evolution of carbonaceous species and dynamic confinement

To further investigate the mechanism behind the selectivity change period, we chose NaFeZr catalyst and NaFeZr-MOR composite catalyst for an in-depth study. Firstly, as shown in Table S4, the N_2 physical adsorption results show that, compared to the pure ZrO_2, the specific surface of the NaFeZr catalyst decreased from 10.5 m^2/g to 9.0 m^2/g and the pore size decreased from 3.7 nm to 3.5 nm before reaction, which may be attributed to the impregnation of Na and Fe elements into the pore channel and forming Fe_2O_3 particles, leading to a slight decrease in pore size and specific surface. Furthermore, the TEM image of the spent NaFeZr catalyst, as shown in Fig. 2(a, b, c), we can see the pore structure of the ZrO_2 support in the yellow circle region, and corresponding inverse fast Fourier transform (IFFT) analysis show the presence of Fe_5C_2 phase in this region, which is generally considered as the active phase for C-C coupling [46–48], suggesting that Na and Fe elements impregnated into the pore channel and undergone oxidation and corresponding carbonization during the preparation and reaction, which is consistent with previous studies[12,49], XRD spectra shown in Fig. S8 also confirms this result, for the catalyst of Fresh and Reduction, Fe_2O_3 (JCPDS, 01–1053) and Fe (JCPDS,25–1408) phase were observed. On the other hand, we conducted the TPH on NaFeZr catalysts after different reaction time, the results are shown in Fig. 3a. It could be seen that the peak intensity of CH_4 ($m/z = 16$) increased with the reaction time prolonging, and the temperature corresponding to the peak rose a little, indicating that the longer the reaction time, the heavier carbonaceous species accumulated in the pore of ZrO_2 support. Based on the above, we infer that the selectivity change period of NaFeZr catalysts is attributed to the confinement nature of the ZrO_2 pores, resulting in the effective diffusion space and pore size contracted, which leads to the difference in diffusion behavior of products owing to different sizes, further, light molecules are more likely to diffuse out, thus leading to more $C_{2-4}^{=}$ and less C_{5+}.

As shown in Table S2, when the NaFeZr catalyst coupled with the MOR, the selectivity of $C_{2-4}^{=}$ grows almost from 0 during the selectivity change period, its selectivity is higher than NaFeZr catalyst alone, it's clear that this change should be attributed to the addition of zeolite. And we can notice that the selectivity of light alkanes (C_{2-4}°) is very high at the beginning of the reaction. Table S5 shows the results of N_2 physical adsorption of fresh and spent MOR with undergoing different reaction times. It could be seen that the specific surface area of zeolite from 422.4 m^2/g decreasing to 40.3 m^2/g (TOS=3 h), with reaction time prolonging, both specific surface and pore volume keeping decrease continuously. Many studies have shown that the acidity of zeolite can cause hydrogenation and cracking of hydrocarbons, and the carbon deposition cover the acidic sites to inactivate the zeolite.[50,51] We speculate that a similar process occurs in MOR.

To investigate the reason, we also conducting TPH on MOR that experience different reaction times, the results are shown in Fig. 3b, similar to the NaFeZr catalyst, the area of the methane ($m/z = 16$) peak became larger and larger with increasing reaction time, and the temperature corresponding to the peak clearly increased, which indicates that the amount of carbon deposition in the MOR pore channel is increasing, and there is a tendency for the accumulated carbonaceous species to evolve to heavy carbonaceous species. Previous studies have also noted the carbon accumulation in MOR during the reaction of CO_2 hydrogenation to light olefins, however, they were limited to the static zeolite after reaction [26].

Meanwhile, as shown in Fig. 4d of *In situ* DRIFTS, the absorption intensity of the peaks in the region of wave number between 3550 cm^{-1} and 3650 cm^{-1} continues to decrease, which corresponds to the hydroxyl vibrational bands in the Si-OH-Al region [28,52], Namely, with reaction time prolonging, the number of Brønsted acid sites show a downward trend, at the same time, the results of Py-IR also confirm this point presented in Fig. S9. Therefore, the acidic sites in the MOR pore channel cause hydrogenation or cracking of hydrocarbon products generated on the NaFeZr catalyst. Further, the amount of carbon deposition increased as a result of cracking, which led to the deactivation of the acidic sites and the gradual blockage of the pore channel, resulting in the continuous decrease of the specific surface area and pore volume of the MOR.(Table S5) Also, as presented in Fig. 2, the HAADF-TEM image show that compared to fresh MOR (g, h, i, j), the amounts of carbonaceous species of spent MOR (k, l, m, n) is much more while other elements keep almost no change, indicating more carbon deposition lied in the spent MOR, and the morphology of the MOR keep stable after reaction (d, e, f).

Furthermore, the areas under TPH curve of Fig. 3b that on behalf of the carbonaceous species amounts to some extent, were calculated by integrating, which correlated with the surface area and micropore volume shown in Table S5, the results were presented in Fig. 5. In addition, a descriptor was defined to describe the free space of MOR micropore channel during the selectivity change period, called 'free space coefficient' (FSC). Assuming the micropores channel were filled completely with the carbonaceous species, as shown in Fig. 5, the micropore volume curve was extrapolated to zero, which will get a percentage of 10 wt%. Thus, the percentage of occupied space by carbonaceous species in MOR

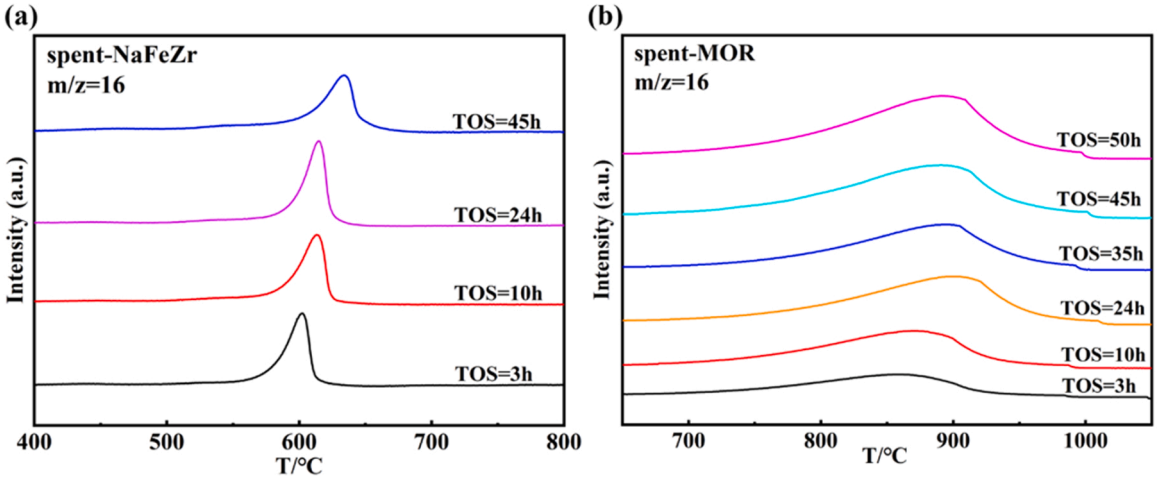

Fig. 3. TPH curve of spent NaFeZr catalyst (a) with time on stream of 3 h, 10 h, 24 h, 45 h and spent MOR (b) with time on stream of 3 h, 10 h, 24 h, 35 h, 45 h, 50 h, respectively.

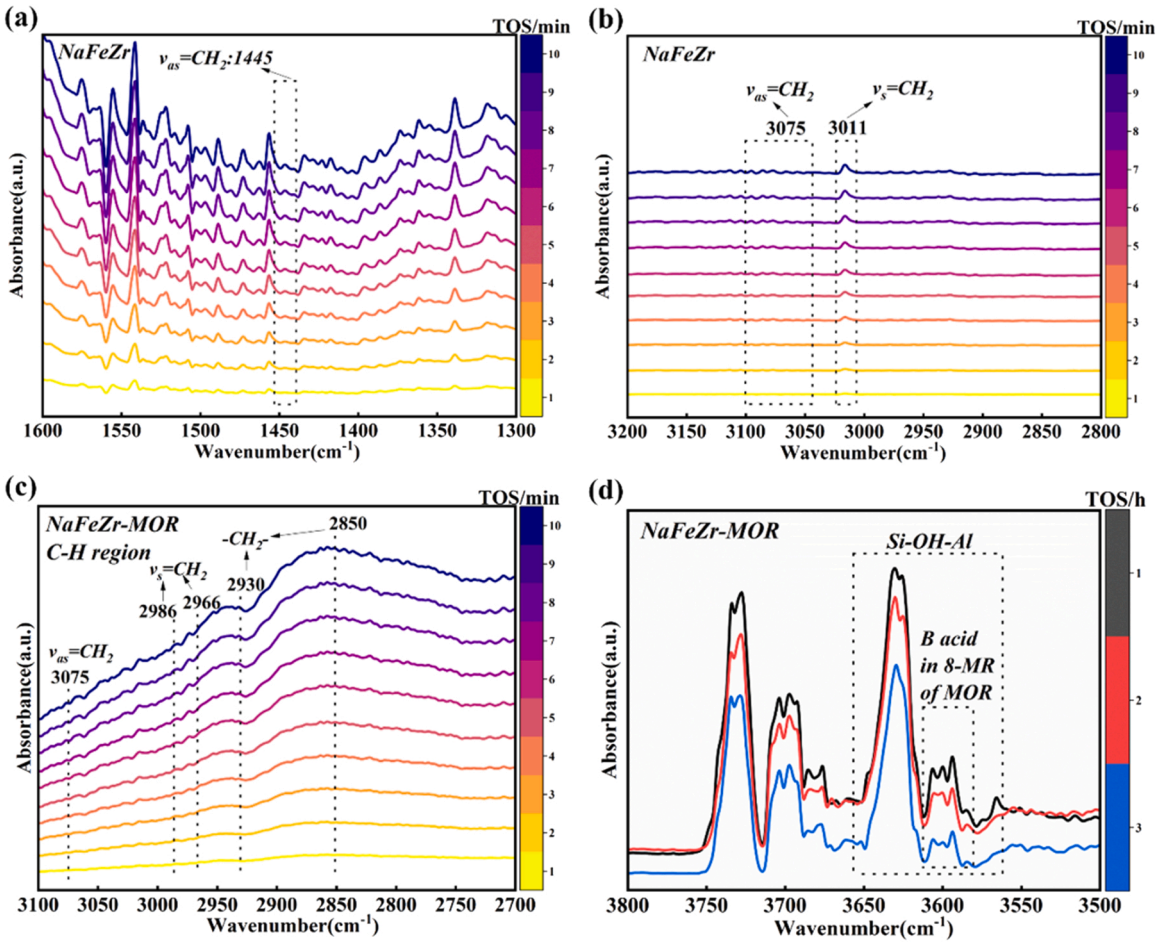

Fig. 4. *In situ* DRIFT spectra of NaFeZr (a)~(b) and NaFeZr-MOR (c)~(d) on CO_2 hydrogenation to light olefins at 0.1 MPa, 320 °C.

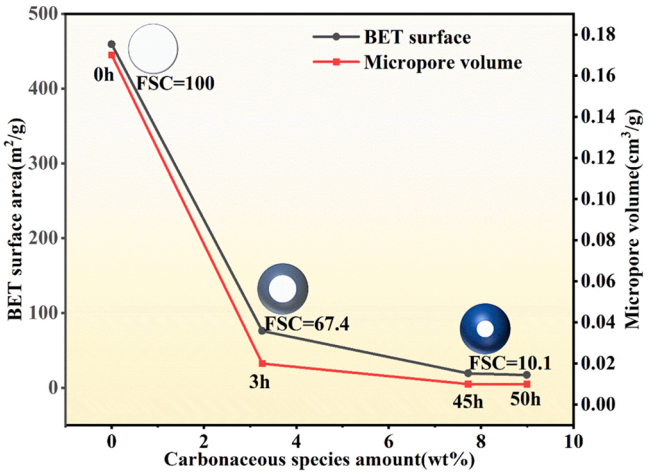

Fig. 5. Correlation of BET surface area and micropore volume with carbonaceous species amount.

micropore at a certain reaction time (t), was estimated by formulation in the Supplementary Information of calculation of FSC. With reaction time increasing, the more the carbon deposition amount, the less free space in MOR micropores channel, namely, the value of FSC decreased continuously. Meanwhile, as shown in Fig. 6, the gas chromatography-mass spectrometer (GC-MS) further demonstrating that carbonaceous deposition species evolved from more light chain hydrocarbons to monocyclic and polycyclic aromatic hydrocarbons with the reaction

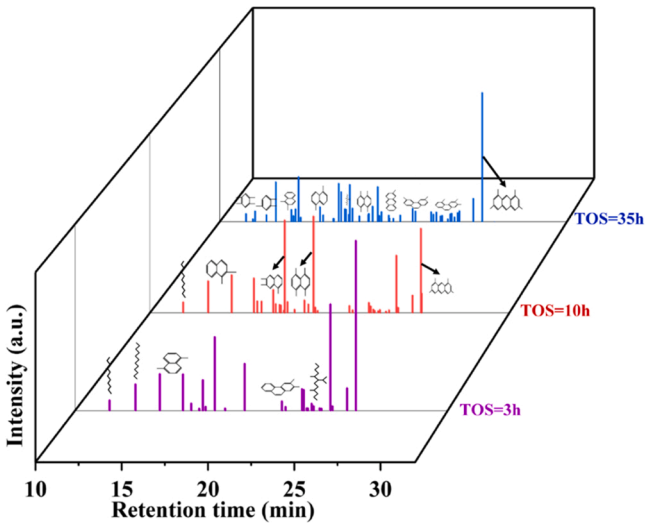

Fig. 6. GC-MS spectra of spent MOR with time on stream of 3 h, 10 h, 35 h, respectively.

proceeding.

Based on above, we can deduce that the pore blockage and the evolution of carbon deposition to heavy carbonaceous species, which eventually reduce the effective mass transfer space in the MOR pores, leading to dynamic changes in diffusion behavior of product molecules and selectivity, and before this dynamic reach equilibrium, a selectivity

change period was created and existed, that is "dynamic confinement". Recently, a similar concept was proposed by Wang et al. in the context of syngas catalytic conversion with ketene as intermediates.[53] Thus, the hydrogenation of light olefins and the cleavage of heavy carbon hydrocarbons by the acidity of MOR at the beginning of the reaction, resulting in a high selectivity for light alkanes (C_{2-4}^{o}), while the selectivity for C_{5+} undergoes a rapid increase from a smaller value and then decreases during the selectivity change period. At the same time, as shown in Fig. S6, there are almost no lower olefins when the basic active sites catalyst (such as the NaFeZr) and the acidic active sites catalyst (such as the MOR) were filled in a very close configuration of Powder-mixing, which could origin from the basic and the acidic active sites poison each other, leading to deactivate for the whole catalyst, this point was proved by previous study [12].

Generally, zeolites are shape-selective due to their inherent structure [24,27,29]. However, the XRD spectra of Fig. S10 shows that there is almost no difference in the crystal structure between the MOR before and after different reaction times, which indicating that the dynamic confinement should not be attributed to the topology of the MOR. Subsequently, we performed in situ DRIFTS characterization of NaFeZr and NaFeZr-MOR, respectively. For the NaFeZr-MOR, as shown in Fig. 4**c**, it can be observed that the intensity of the absorption peak gradually increases along time in the region of wave number 2700 cm^{-1} to 3100 cm^{-1}, which usually corresponds to the stretching vibration region of the C-H bond [24,52]. For the NaFeZr catalyst, the intensity of the absorption peaks located C-H region does not increase significantly, except for the peak at wave number 3011 cm^{-1} and 3075 cm^{-1} (Fig. 4b), as well as the peak at wave number 1445 cm^{-1} (Fig. 4a), the three peaks often correspond to the symmetrical or asymmetrical stretching vibration of $=CH_2$ bonds.[54–56] Indicating that only a small amount accumulation of carbon species in the support pore, which proves that the selectivity change period of NaFeZr catalyst is more from the confinement effect of the support pore channel; while for NaFeZr-MOR composite catalyst, the presence of acidic sites in the MOR micropores channel aggravates the carbon deposition and the evolution to heavy carbonaceous species, leading to the "dynamic confinement" during the selectivity change period, which is consistent with the above deduction.

Two key points observed here are confinement of the ZrO_2 support and the carbon deposition in MOR channel. On the one hand, for the confinement of ZrO_2, we adopted a modification method blocking the ZrO_2 support pore channel, preparing NaFeZr (blockage) catalysts with small specific surface and NaFeZr(HT) catalysts with large specific surface (Table S4). The reaction performance is shown in Table S6, as can be seen, although the selectivity of $C_{2-4}^{=}$ remained almost unchanged, the conversion of CO_2 decreased as well as the selectivity of CO showed a high growth, indicating that the Na and Fe of the NaFeZr (blockage) did not enter the support pores due to blocking, thus significantly reducing the confinement effect of the pores, resulting in sintering of surface active phase while reducing the number of active sites, which in agreement with previous studies [21]. For the NaFeZr(HT), as shown in Fig. S11, the products were dominated by light alkane (C_{2-4}^{o}), because when the pore size or specific surface was more large, although the active components impregnated into the channel, the more large space also caused secondary hydrogenation of light olefins, suggesting the important influence of the support itself on the confinement effect, which is similar with previous studies [17].

On the other hand, a single feed gas of 1-C_6H_{12} to MOR alone is used to discuss the carbon deposition in the pore channels caused by the MOR (Table S7). It is easy to see that at the beginning of the reaction, the MOR present effective cracking on 1-C_6H_{12}, as well as hydrogenation, thus producing 0.7% light olefins ($C_{2-4}^{=}$), and 75% light alkanes (C_{2-4}^{o}) with isobutane as the major product (53.6%). The MOR has excellent ability to crack light hydrocarbons, and isobutane is the main products, which is consistent with the previous study [26]. With reaction time increasing to 2.7 h, when the pore acidic sites were gradually deactivated due to a large amount of carbon deposition, the cleavage of MOR gradually weakened, and the selectivity of C_{5+} jumped from 24.3% to 88.7% and subsequently decreased, the uncracked 1-C_6H_{12} was mainly included here, meanwhile, the selectivity of $C_{2-4}^{=}$ began to gradually and obviously increase. This process is analogous with the above inference of dynamic confinement. So far, we have tested the two key points of the above inference, and confirming the existence of the dynamic confinement again.

However, the process of evolution to more heavy species within the pore channel of MOR cannot go on forever. The one reason is the size limitation of MOR zeolite cage, which cannot contain more heavy species, such as polycyclic aromatic hydrocarbons. More importantly, the presence of hydrogen may also have prevented this process, the hydrogen could participate in the hydrogenolysis of heavy carbonaceous species (coke), which proposed by previous studies.[57,58] So we speculate the hydrogenolysis of coke could reactivate a small number of acidic sites to make the process of evolution to heavy carbonaceous species repeat, which will not lead to the completely blocked of channel pores and finally reaches to steady state. Both the Py-IR spectra in Fig. S9 and the *In situ* DRIFT spectra in Fig. 4d all proved that there is still a small number of acidic sites during the reaction, which is also similar with the relevant study recently.[59].

As shown in Table S7, although there is an increase in the selectivity of $C_{2-4}^{=}$ due to the dynamic confinement, which comes mainly from the growth of propylene ($C_3^{=}$) and butene ($C_4^{=}$), while almost no growth of ethylene ($C_2^{=}$). But, the Fig. 7 shows that the selectivity promotion of $C_{2-4}^{=}$ for the NaFeZr-MOR comes mainly from the increase of ethylene ($C_2^{=}$) compared to the NaFeZr catalyst, indicating that changes in MOR micropores channel during the selectivity change period have different effects on the growth of the respective selectivity of ethylene ($C_2^{=}$), propylene ($C_3^{=}$) and butene ($C_4^{=}$), which we have investigated in depth.

3.3. The role of the 8-MR of MOR in selectivity growth

As well known, MOR possess 12-MR and 8-MR, and there are two types of 8-MR channel structures, namely, the 8-MR that runs parallel to the 12-MR and the 8-MR that acts as a link between the two, the so-called side pocket [28,52]. Among them, the 12-MR as a unidirectional channel, is mainly used for the isomerization and hydrocracking of long-chain hydrocarbons [28,60], which explains the low selectivity of C_{5+} at the beginning of the selectivity change period (Table S2). More importantly, previous mechanism studies have shown that the 8-MR

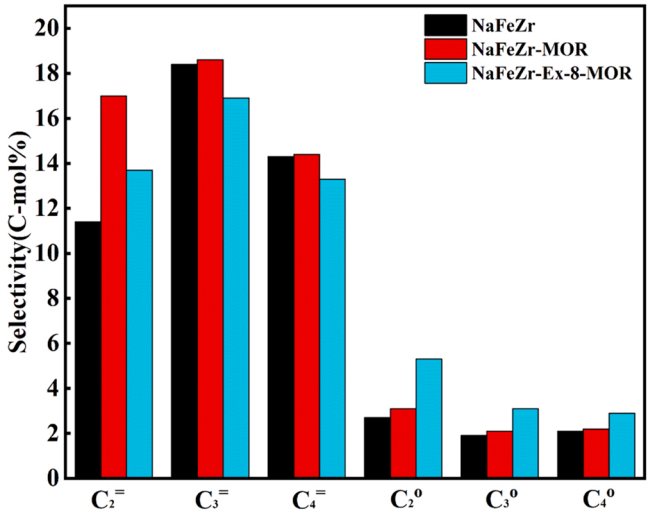

Fig. 7. Selectivity comparison of C_{2-4} species of the NaFeZr, NaFeZr-MOR, NaFeZr-Ex-8-MOR catalyst, respectively. Reaction Conditions: NaFeZr-MOR (weigh ratio=1:3), H_2/CO_2 = 3, P = 3 MPa, GHSV= 9000 $mL \cdot g_{cat}^{-1} \cdot h^{-1}$, T = 320 °C, time on stream, 50 h.

channel of MOR has unique shape-selective catalysis for light olefins, especially ethylene($C_2^=$), for example, the ketene intermediate mechanism [27,28], CO-Formate mechanism have been proposed [26]. These mechanisms is focused on the steady-state reactions or spent catalysts, which we called "steady-state mechanisms". However, we have shown that the increase in $C_{2-4}^=$ selectivity on NaFeZr-MOR during selectivity change period may not be attributed to the shape-selective catalysis from the crystal structure of MOR itself, and this increase is mainly from ethylene ($C_2^=$) selectivity caused by adding MOR compared to NaFeZr catalyst. Furthermore, as seen from the *In situ* DRIFTS spectra of Fig. 4d, the intensity of the absorption peak in the region from 3582 cm^{-1} to 3590 cm^{-1} gradually decreases, which usually corresponding to the Brønsted acid sites of the 8-MR side pocket of MOR(LF)[28], suggesting that the acidity within the 8-MR pore is progressively weakened during the selectivity change period. Hence, based on these results, together with the dynamic confinement already proposed above, we speculate that the increase of ethylene($C_2^=$) selectivity originates from the dynamic confinement of the 8-MR due to carbonaceous accumulation, which is different from the steady-state mechanism.

Many studies have demonstrated that the H+ of Brønsted Acid within the 8-MR can be replaced by Na^+ without affecting the H^+ within the 12-MR [28,36]. Therefore, to further verify the above inference, we performed a shielding operation on the acidic sites for the 8-MR of MOR, (Supplementary Information for details), preparing Ex-8-MOR (The acidic sites of 8-MR in MOR were shielded). Subsequently, we evaluated the NaFeZr-Ex-8-MOR composite catalyst, the results are shown in Table S8. Compared to the NaFeZr-MOR composite catalyst, the reaction process also obviously has a selectivity change period, and the selectivity of C_{5+} undergoes a process similar with that of the NaFeZr-MOR catalyst as the reaction time increases, and remains almost same when reaches the steady state, indicating that the selectivity of C_{5+} still exists the dynamic confinement. (Table S2) Unlike NaFeZr-MOR, despite undergoing a similar growth process, the selectivity of $C_{2-4}^=$ only grows to 44.8 when the reaction reaches the steady state, like the NaFeZr catalyst without adding the MOR, this suggests that the pore acidity of 8-MR has a direct effect on the selectivity of $C_{2-4}^=$. Further, we compare the selectivity of C_2~C_4 species (both alkanes and olefins) for NaFeZr, NaFeZr-MOR, and NaFeZr-Ex-8-MOR, respectively. As shown in Fig. 7, as mentioned above, the selectivity growth of $C_{2-4}^=$ was mainly from the ethylene ($C_2^=$) before shielding the acidic sites of the 8-MR. Interestingly, the selectivity of $C_2^=$, $C_3^=$ and $C_4^=$ decreased while the C_2°, C_3° and C_4° increased after shielding, showing that the reduction of carbon deposition in the 8-MR enlarge the effective diffusion space and facilitate the secondary hydrogenation of $C_{2-4}^=$, this is similar with the previous study [17,53].

To further distinguish and confirm the effect of carbon deposition on diffusion, we define the coefficient ΔS, where S refers to the selectivity of the species, to describe the degree of the change in selectivity. As shown in Table S9, the degree of decrease in olefin selectivity declines with increasing carbon number, while the degree of increase in alkane selectivity also decreases, indicating that the smaller the molecule, the greater the effect of the 8-MR confinement on its diffusion due to carbon deposition. Therefore, with reaction time increasing, when the carbonaceous species accumulation reaches the steady state, the smaller molecules of ethylene ($C_2^=$) are more likely to pass through the confinement pore and enhance the selectivity, which explains why the growth of $C_{2-4}^=$ on the NaFeZr-MOR mainly originates from the growth of ethylene ($C_2^=$), and it is obvious that the dynamic confinement process of C_{5+} occurs more in the 12-MR of MOR.

As well known, the SAPO-34 also has the structure of 8-MR, but its average pore size is 0.38 nm while the MOR is 0.3 nm, and it has a larger cage size than the MOR [34,52], as a result, compared to the SAPO-34, the MOR could provide a more confined environment that suppressed the diffusion of heavy hydrocarbons, that is why the selectivity of $C_{2-4}^=$ is higher for NaFeZr-MOR compared to NaFeZr-SAPO-34 in the final products shown in Fig. S7. Recently, the study also revealed that the moderate acidity strength of zeolite are also important, which could avoid the over hydrogenation for the olefins in the pore channel.[59].

In summary, in the reaction of CO_2 hydrogenation to light olefins, a dynamic confinement process within the pore channel of the MOR due to carbon deposition occurred on the NaFeZr-MOR. As the reaction time increases, the dynamic confinement within the 8-MR pore channel allows the diffusion and passage for more small molecules, which enhances the selectivity of $C_{2-4}^=$ especially for ethylene ($C_2^=$).

Finally, compared to the similar catalysts in literature already reported, the synthesis processes of NaFeZr-MOR are simple relatively. Meanwhile, in order to test the "dynamic confinement" presented in this paper again, which shown in Fig. 8, we prepare coprecipitation catalyst, NaFe and NaFe-MOR, which quote the catalyst previously reported by our group, the FeNa(1.18) catalyst [37]. The results are shown in Tables S10 and S11, compared to the NaFe, the NaFe-MOR composite catalyst clearly has a selectivity change period, that is, dynamic confinement process, which coinciding with the above and proving its universality.

4. Conclusions

In this paper, we report an iron-based composite catalyst, NaFeZr-MOR, and reveal its dynamic confinement effect. We found that both the NaFeZr catalyst alone and the NaFeZr-MOR composite catalyst have an obvious selectivity change period. For the NaFeZr-MOR, the selectivity of $C_{2-4}^=$ rises continuously to over 51% (Table S3) with increasing reaction time, while the selectivity of C_{5+} undergoes a brief rise and then keeps falling to below 28%. A similar phenomenon was found in other supported catalysts coupled with the same or similar zeolites. Subsequently, in-depth characterization of NaFeZr-MOR composite catalysts reveals that the essence of the selectivity change period is the accumulation and evolution of the carbonaceous species, which caused a gradual increase for the channel confinement effect, namely, this is a dynamic confinement process. This process brings about the changes on the diffusion behavior of product molecules, which directly lead to the alteration for the product selectivity. Based on this, we conclude that the 8-MR of MOR is beneficial to enhance the selectivity of light olefins especially for ethylene($C_2^=$) is more due to the difference in the diffusion behavior of small molecules, which caused by the dynamic confinement process of its channel. These findings may provide new insights and guidance for the catalyst design involving CO_2/CO hydrogenation and the selectivity regulation of products in the future.

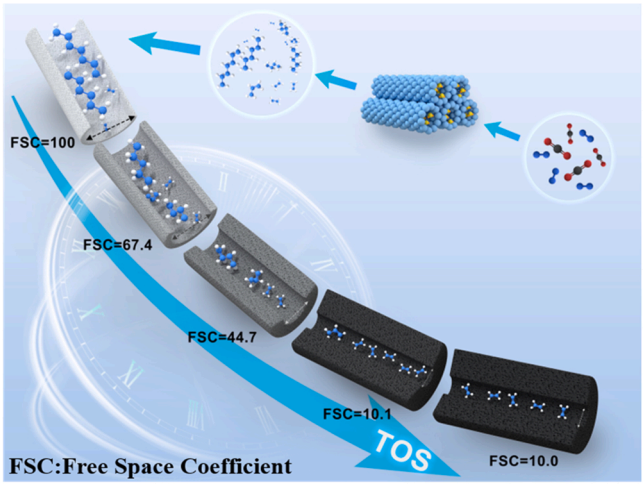

Fig. 8. Schematic of the dynamic confinement process in CO_2 hydrogenation to light olefins on NaFeZr-MOR.

CRediT authorship contribution statement

J.S. conceived and designed this work. L.W. wrote the manuscript. L. W. and Y.H. synthesized, characterized, and evaluated the catalysts. J. W., S.L., Y. M. and Q.G. participated in the analysis and discussion of the experimental data. J.S. and Q.G. supervised the whole project.

Declaration of Competing Interest

The authors declare that they have no known competing financial interests or personal relationships that could have appeared to influence the work reported in this paper.

Data Availability

Data will be made available on request.

Acknowledgements

The authors would like to thank the support of National Key Research and Development Program of China (2022YFA1604101, 2022YFA1504702), National Natural Science Foundation of China (22078315, 22172169), Liaoning BaiQianWan Talents Program, Liaoning Revitalization Talents Program (No. XLYC1907066) and DICP (Grant: DICP I202012).

Supplementary Material

The Supplementary Material includes additional experimental details of characterizations and catalytic results, Figs. S1-S11 and Table S1-S11.

Appendix A. Supporting information

Supplementary data associated with this article can be found in the online version at doi:10.1016/j.apcatb.2023.122506.

References

[1] U. Rodemerck, M. Holeňa, E. Wagner, Q. Smejkal, A. Barkschat, M. Baerns, Catalyst development for CO_2 hydrogenation to fuels, ChemCatChem 5 (2013) 1948–1955.
[2] M.D. Porosoff, B. Yan, J.G. Chen, Catalytic reduction of CO_2 by H2 for synthesis of CO, methanol and hydrocarbons: challenges and opportunities, Energy Environ. Sci. 9 (2016) 62–73.
[3] D. Fu, M.E. Davis, Carbon dioxide capture with zeotype materials, Chem. Soc. Rev. (2022).
[4] M. Aresta, A. Dibenedetto, A. Angelini, The changing paradigm in CO_2 utilization, J. CO_2 Util. 3–4 (2013) 65–73.
[5] X.-H. Liu, J.-G. Ma, Z. Niu, G.-M. Yang, P. Cheng, An efficient nanoscale heterogeneous catalyst for the capture and conversion of carbon dioxide at ambient pressure, Angew. Chem. Int. Ed. 54 (2015) 988–991.
[6] Q. Liu, L. Wu, R. Jackstell, M. Beller, Using carbon dioxide as a building block in organic synthesis, Nat. Commun. 6 (2015) 5933.
[7] L.O. Amberg, A.E. Robinson, Ethylene—propylene rubber, Ind. Eng. Chem. 53 (1961) 368–370.
[8] P.P. McClellan, Manufacture and uses of ethylene oxide and ethylene glycol, Ind. Eng. Chem. 42 (1950) 2402–2407.
[9] G. Centi, E.A. Quadrelli, S. Perathoner, Catalysis for CO_2 conversion: a key technology for rapid introduction of renewable energy in the value chain of chemical industries, Energy Environ. Sci. 6 (2013) 1711–1731.
[10] T. Ren, M. Patel, K. Blok, Olefins from conventional and heavy feedstocks: Energy use in steam cracking and alternative processes, Energy 31 (2006) 425–451.
[11] T. Ren, M.K. Patel, K. Blok, Steam cracking and methane to olefins: Energy use, CO_2 emissions and production costs, Energy 33 (2008) 817–833.
[12] J. Wei, Q. Ge, R. Yao, Z. Wen, C. Fang, L. Guo, H. Xu, J. Sun, Directly converting CO_2 into a gasoline fuel, Nature, Communications 8 (2017) 15174.
[13] N. Lohitharn, J.G. Goodwin, E. Lotero, Fe-based Fischer–Tropsch synthesis catalysts containing carbide-forming transition metal promoters, J. Catal. 255 (2008) 104–113.
[14] P.S. Sai Prasad, J.W. Bae, K.-W. Jun, K.-W. Lee, Fischer–Tropsch synthesis by carbon dioxide hydrogenation on Fe-Based catalysts, Catal. Surv. Asia 12 (2008) 170–183.
[15] W. Zhou, K. Cheng, J. Kang, C. Zhou, V. Subramanian, Q. Zhang, Y. Wang, New horizon in C1 chemistry: breaking the selectivity limitation in transformation of syngas and hydrogenation of CO_2 into hydrocarbon chemicals and fuels, Chem. Soc. Rev. 48 (2019) 3193–3228.
[16] C. Dai, A. Zhang, M. Liu, J. Li, F. Song, C. Song, X. Guo, Facile one-step synthesis of hierarchical porous carbon monoliths as superior supports of Fe-based catalysts for CO_2 hydrogenation, RSC Adv. 6 (2016) 10831–10836.
[17] S. Hu, M. Liu, F. Ding, C. Song, G. Zhang, X. Guo, Hydrothermally stable MOFs for CO_2 hydrogenation over iron-based catalyst to light olefins, J. CO_2 Util. 15 (2016) 89–95.
[18] S. Wang, T. Wu, J. Lin, Y. Ji, S. Yan, Y. Pei, S. Xie, B. Zong, M. Qiao, Iron–potassium on single-walled carbon nanotubes as efficient catalyst for CO_2 hydrogenation to heavy olefins, ACS Catal. 10 (2020) 6389–6401.
[19] A. Ramirez, L. Gevers, A. Bavykina, S. Ould-Chikh, J. Gascon, Metal organic framework-derived iron catalysts for the direct hydrogenation of CO_2 to short chain olefins, ACS Catal. 8 (2018) 9174–9182.
[20] P. Zhang, F. Han, J. Yan, X. Qiao, Q. Guan, W. Li, N-doped ordered mesoporous carbon (N-OMC) confined Fe3O4-FeCx heterojunction for efficient conversion of CO_2 to light olefins, Appl. Catal. B: Environ. 299 (2021), 120639.
[21] T. Wu, J. Lin, Y. Cheng, J. Tian, S. Wang, S. Xie, Y. Pei, S. Yan, M. Qiao, H. Xu, B. Zong, Porous graphene-confined Fe–K as highly efficient catalyst for CO_2 direct hydrogenation to light olefins, ACS Appl. Mater. Interfaces 10 (2018) 23439–23443.
[22] Y. Li, L. Zeng, G. Pang, X. Wei, M. Wang, K. Cheng, J. Kang, J.M. Serra, Q. Zhang, Y. Wang, Direct conversion of carbon dioxide into liquid fuels and chemicals by coupling green hydrogen at high temperature, Appl. Catal. B: Environ. 324 (2023), 122299.
[23] P. Gao, S. Dang, S. Li, X. Bu, Z. Liu, M. Qiu, C. Yang, H. Wang, L. Zhong, Y. Han, Q. Liu, W. Wei, Y. Sun, Direct production of lower olefins from CO_2 conversion via bifunctional catalysis, ACS Catal. 8 (2018) 571–578.
[24] X. Liu, M. Wang, H. Yin, J. Hu, K. Cheng, J. Kang, Q. Zhang, Y. Wang, Tandem catalysis for hydrogenation of CO and CO_2 to lower olefins with bifunctional catalysts composed of spinel oxide and SAPO-34, ACS Catal. 10 (2020) 8303–8314.
[25] Z. Li, J. Wang, Y. Qu, H. Liu, C. Tang, S. Miao, Z. Feng, H. An, C. Li, Highly selective conversion of carbon dioxide to lower olefins, ACS Catal. 7 (2017) 8544–8548.
[26] A. Ramirez, A. Dutta Chowdhury, A. Dokania, P. Cnudde, M. Caglayan, I. Yarulina, E. Abou-Hamad, L. Gevers, S. Ould-Chikh, K. De Wispelaere, V. van Speybroeck, J. Gascon, Effect of zeolite topology and reactor configuration on the direct conversion of CO_2 to light olefins and aromatics, ACS Catal. 9 (2019) 6320–6334.
[27] F. Jiao, J. Li, X. Pan, J. Xiao, H. Li, H. Ma, M. Wei, Y. Pan, Z. Zhou, M. Li, S. Miao, J. Li, Y. Zhu, D. Xiao, T. He, J. Yang, F. Qi, Q. Fu, X. Bao, Selective conversion of syngas to light olefins, Science 351 (2016) 1065–1068.
[28] F. Jiao, X. Pan, K. Gong, Y. Chen, G. Li, X. Bao, Shape-selective zeolites promote ethylene formation from syngas via a ketene intermediate, Angew. Chem. Int. Ed. 57 (2018) 4692–4696.
[29] P. Gao, S. Li, X. Bu, S. Dang, Z. Liu, H. Wang, L. Zhong, M. Qiu, C. Yang, J. Cai, W. Wei, Y. Sun, Direct conversion of CO_2 into liquid fuels with high selectivity over a bifunctional catalyst, Nat. Chem. 9 (2017) 1019–1024.
[30] Y. Ding, F. Jiao, X. Pan, X. Bao, Modulated hydrocarbon distribution of gasoline deriving from butene conversion in the presence of syngas, J. Energy Chem. 73 (2022) 416–421.
[31] W. Gao, L. Guo, Q. Wu, C. Wang, X. Guo, Y. He, P. Zhang, G. Yang, G. Liu, J. Wu, N. Tsubaki, Capsule-like zeolite catalyst fabricated by solvent-free strategy for para-Xylene formation from CO_2 hydrogenation, Appl. Catal. B: Environ. 303 (2022), 120906.
[32] N. Li, F. Jiao, X. Pan, Y. Chen, J. Feng, G. Li, X. Bao, High-quality gasoline directly from syngas by dual metal oxide–zeolite (OX-ZEO) catalysis, Angew. Chem. Int. Ed. 58 (2019) 7400–7404.
[33] J. Yang, K. Gong, D. Miao, F. Jiao, X. Pan, X. Meng, F. Xiao, X. Bao, Enhanced aromatic selectivity by the sheet-like ZSM-5 in syngas conversion, J. Energy Chem. 35 (2019) 44–48.
[34] S. Rimaz, M. Kosari, M. Zarinejad, S. Ramakrishna, A comprehensive review on sustainability-motivated applications of SAPO-34 molecular sieve, J. Mater. Sci. 57 (2022) 848–886.
[35] A. Ramirez, X. Gong, M. Caglayan, S.-A.F. Nastase, E. Abou-Hamad, L. Gevers, L. Cavallo, A. Dutta Chowdhury, J. Gascon, Selectivity descriptors for the direct hydrogenation of CO_2 to hydrocarbons during zeolite-mediated bifunctional catalysis, Nat. Commun. 12 (2021) 5914.
[36] A. Bhan, A.D. Allian, G.J. Sunley, D.J. Law, E. Iglesia, Specificity of sites within eight-membered ring zeolite channels for carbonylation of methyls to acetyls, J. Am. Chem. Soc. 129 (2007) 4919–4924.
[37] J. Wei, J. Sun, Z. Wen, C. Fang, Q. Ge, H. Xu, New insights into the effect of sodium on Fe3O4- based nanocatalysts for CO_2 hydrogenation to light olefins, Catal. Sci. Technol. 6 (2016) 4786–4793.
[38] K. Li, J.G. Chen, CO_2 hydrogenation to methanol over ZrO2-containing catalysts: insights into ZrO2 induced synergy, ACS Catal. 9 (2019) 7840–7861.
[39] J. Wang, Z. You, Q. Zhang, W. Deng, Y. Wang, Synthesis of lower olefins by hydrogenation of carbon dioxide over supported iron catalysts, Catal. Today 215 (2013) 186–193.
[40] W. Li, X. Nie, X. Jiang, A. Zhang, F. Ding, M. Liu, Z. Liu, X. Guo, C. Song, ZrO2 support imparts superior activity and stability of Co catalysts for CO_2 methanation, Appl. Catal. B: Environ. 220 (2018) 397–408.
[41] B. Liang, H. Duan, T. Sun, J. Ma, X. Liu, J. Xu, X. Su, Y. Huang, T. Zhang, Effect of Na promoter on Fe-based catalyst for CO_2 hydrogenation to alkenes, ACS Sustain. Chem. Eng. 7 (2019) 925–932.
[42] Q. Yang, V.A. Kondratenko, S.A. Petrov, D.E. Doronkin, E. Saraçi, H. Lund, A. Arinchtein, R. Kraehnert, A.S. Skrypnik, A.A. Matvienko, E.V. Kondratenko,

Identifying performance descriptors in CO_2 hydrogenation over iron-based catalysts promoted with alkali metals, Angew. Chem. Int. Ed. 61 (2022), e202116517.
[43] S. Zhang, Z. Wu, X. Liu, Z. Shao, L. Xia, L. Zhong, H. Wang, Y. Sun, Tuning the interaction between Na and Co2C to promote selective CO_2 hydrogenation to ethanol, Appl. Catal. B: Environ. 293 (2021), 120207.
[44] H. Suo, S. Wang, C. Zhang, J. Xu, B. Wu, Y. Yang, H. Xiang, Y.-W. Li, Chemical and structural effects of silica in iron-based Fischer–Tropsch synthesis catalysts, J. Catal. 286 (2012) 111–123.
[45] T. Xie, J. Wang, F. Ding, A. Zhang, W. Li, X. Guo, C. Song, CO_2 hydrogenation to hydrocarbons over alumina-supported iron catalyst: Effect of support pore size, J. CO_2 Util. 19 (2017) 202–208.
[46] C. Yang, H.B. Zhao, Y.L. Hou, D. Ma, Fe5C2 nanoparticles: a facile bromide-induced synthesis and as an active phase for fischer-tropsch synthesis, J. Am. Chem. Soc. 134 (2012) 15814–15821.
[47] T.H. Pham, Y. Qi, J. Yang, X. Duan, G. Qian, X. Zhou, D. Chen, W. Yuan, Insights into Hägg iron-carbide-catalyzed fischer–tropsch synthesis: suppression of CH4 formation and enhancement of C–C coupling on χ-Fe5C2 (510), ACS Catal. 5 (2015) 2203–2208.
[48] X. Liu, J. Liu, Y. Yang, Y.-W. Li, X. Wen, Theoretical Perspectives on the Modulation of Carbon on Transition-Metal Catalysts for Conversion of Carbon-Containing Resources, ACS Catal. 11 (2021) 2156–2181.
[49] S. Wang, Y. Ji, X. Liu, S. Yan, S. Xie, Y. Pei, H. Li, M. Qiao, B. Zong, Potassium as a Versatile Promoter to Tailor the Distribution of the Olefins in CO Hydrogenation over Iron-Based Catalyst, ChemCatChem (2022).
[50] H. Tian, J. Yao, F. Zha, L. Yao, Y. Chang, Catalytic activity of SAPO-34 molecular sieves prepared by using palygorskite in the synthesis of light olefins via CO_2 hydrogenation, Appl. Clay Sci. 184 (2020), 105392.
[51] X. Zhang, A. Zhang, X. Jiang, J. Zhu, J. Liu, J. Li, G. Zhang, C. Song, X. Guo, Utilization of CO_2 for aromatics production over ZnO/ZrO2-ZSM-5 tandem catalyst, J. CO_2 Util. 29 (2019) 140–145.
[52] R. Liu, S. Zeng, T. Sun, S. Xu, Z. Yu, Y. Wei, Z. Liu, Selective removal of acid sites in mordenite zeolite by trimethylchlorosilane silylation to improve dimethyl ether carbonylation stability, ACS Catal. 12 (2022) 4491–4500.
[53] H. Wang, F. Jiao, Y. Ding, W. Liu, Z. Xu, X. Pan, X. Bao, Dynamic confinement of SAPO-17 cage on the selectivity control of syngas conversion, Natl. Sci. Rev. (2022).
[54] W. Ji, Y. Chen, S. Shen, S. Li, H. Wang, FTIR study of adsorption of CO, NO and C2H4 and reaction of CO + H2 on the well-dispersed FeOxγ-Al2O3 and FeOxTiO2 (a) catalysts, Appl. Surf. Sci. 99 (1996) 151–160.
[55] A.A. Efremov, A.A. Davydov, Infrared spectra of π-complexes of propylene and ethylene on TiO2, React. Kinet. Catal. Lett. 15 (1980) 327–331.
[56] H. Leclerc, A. Vimont, J.-C. Lavalley, M. Daturi, A.D. Wiersum, P.L. Llwellyn, P. Horcajada, G. Férey, C. Serre, Infrared study of the influence of reducible iron (iii) metal sites on the adsorption of CO, CO_2, propane, propene and propyne in the mesoporous metal–organic framework MIL-100, Phys. Chem. Chem. Phys. 13 (2011) 11748–11756.
[57] S.S. Arora, D.L.S. Nieskens, A. Malek, A. Bhan, Lifetime improvement in methanol-to-olefins catalysis over chabazite materials by high-pressure H2 co-feeds, Nat. Catal. 1 (2018) 666–672.
[58] X. Zhao, J. Li, P. Tian, L. Wang, X. Li, S. Lin, X. Guo, Z. Liu, Achieving a superlong lifetime in the zeolite-catalyzed MTO reaction under high pressure: synergistic effect of hydrogen and water, ACS Catal. 9 (2019) 3017–3025.
[59] S. Wang, L. Zhang, P. Wang, W. Jiao, Z. Qin, M. Dong, J. Wang, U. Olsbye, W. Fan, Highly selective hydrogenation of CO_2 to propane over GaZrOx/H-SSZ-13 composite, Nat. Catal. (2022).
[60] A. Chica, A. Corma, Hydroisomerization of pentane, hexane, and heptane for improving the octane number of gasoline, J. Catal. 187 (1999) 167–176.